Assorbanza ottica

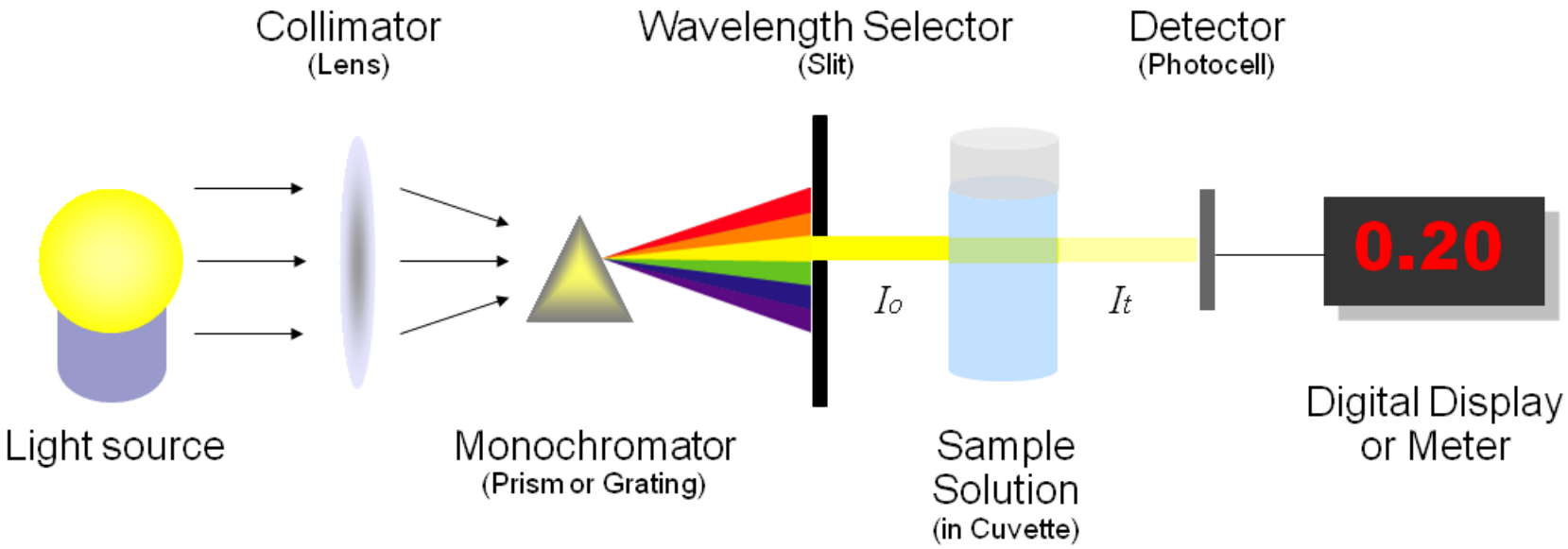

Trasmittanza ottica : $T(\lambda) = \frac{I_t(\lambda)}{I_0(\lambda)}$

Assorbanza ottica : $A(\lambda) = log\left(\frac{I_0(\lambda)}{I_t(\lambda)}\right) = -\log(T(\lambda))$

$I_0\ (\lambda)$ = intensità della luce incidente

$I_t\ (\lambda)$ = intensità della luce trasmessa

TRANSIZIONI OTTICHE

SEMICONDUTTORE

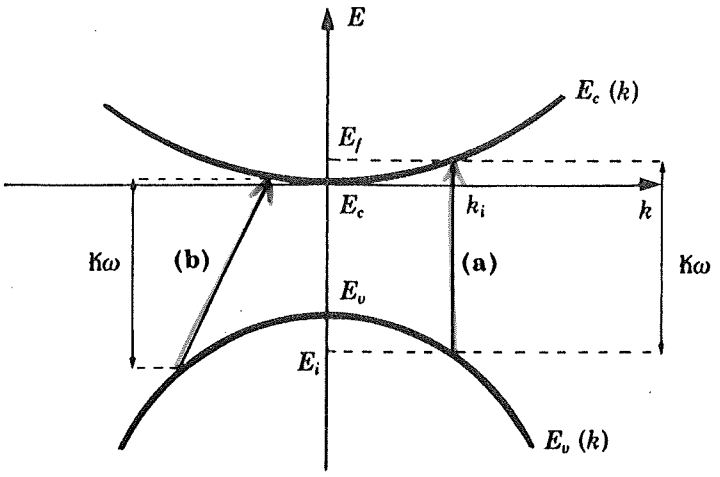

Fig. 6.2. Direct (a) and indirect (b) absorption in a semiconductor.

$\bar{k}_i = \bar{k}_f$ $\quad \bar{k}_i + \bar{q} = \bar{k}_f$

METALLO

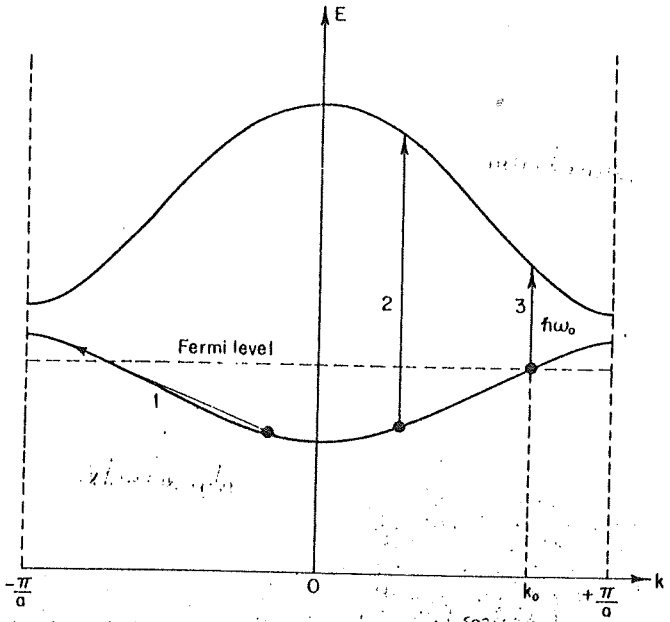

Fig. 3.14 A schematic band diagram for a metal. The threshold for direct transitions is from the Fermi energy at $\mathbf{k}_0$ to the same state $\mathbf{k}_0$ in the next higher band.

METALLO CON BANDA d

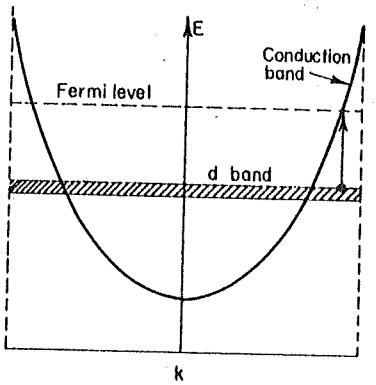

Fig. 3.16 Schematic band diagram for the noble metals.

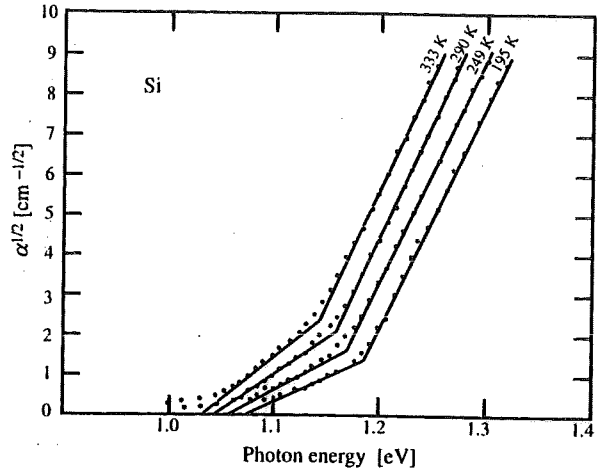

Fig. 6.17. Plots of the square root of the absorption coefficients of Si versus photon energy at several temperatures. The two segments of a straight line drawn through the experimental points represent the two contributions due to phonon absorption and emission [6.26]

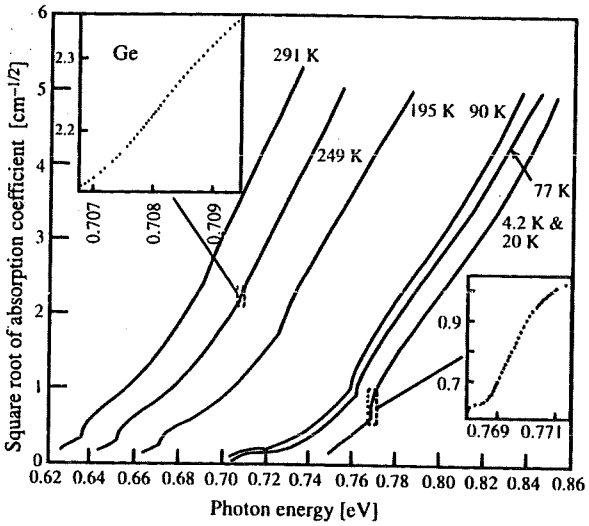

Fig. 6.18. Plots of the square root of the absorption coefficients of Ge versus photon energy at several temperatures. The two *insets* compare the exciton-induced abruptness of the absorption edge due to phonon emission at high and low temperatures [6.27]

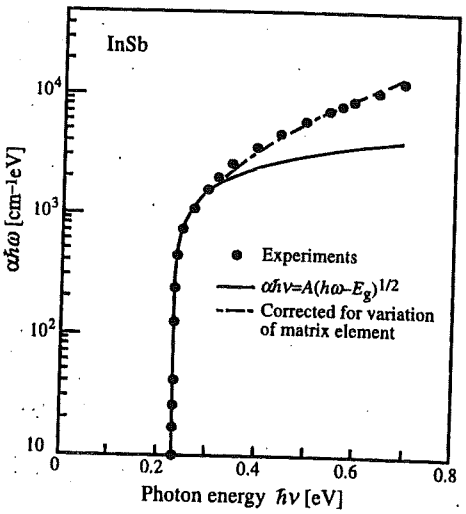

Fig. 6.15. Semilogarithmic plot of the absorption coefficient of InSb at 5 K as a function of photon energy. The *filled circles* represent experimental results from [6.24]. The *curves* have been calculated using various models. The intercept with the x-axis gives the direct bandgap of InSb [6.25]

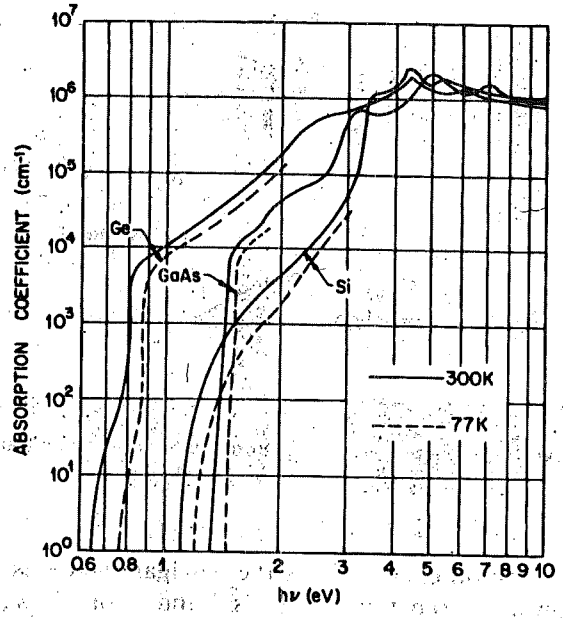

Fig. 27 Measured absorption coefficients near and above the fundamental absorption edge for pure Ge, Si, and GaAs. (After Dash and Newman, Ref. 51; Philipp and Taft, Ref. 52; Hill, Ref. 53; Casey, Sell, and Wecht, Ref. 54.)

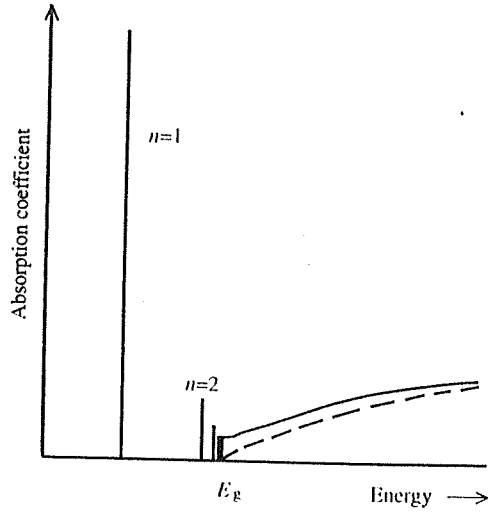

Fig. 6.24. Comparison between the absorption spectra in the vicinity of the bandgap of a direct-gap semiconductor with (*solid lines*) and without (*broken curve*) exciton effects

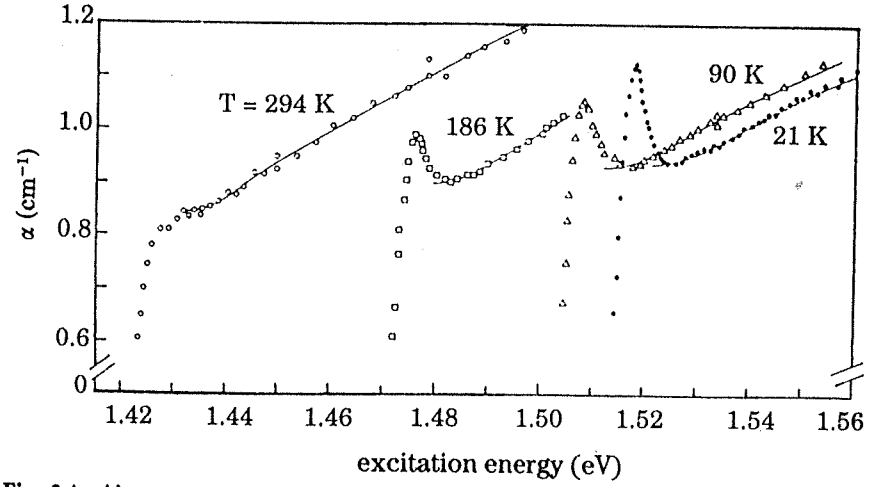

GaAs

$E_g = 1.52$ eV (~0K)

Fig. 6.4. Absorption in GaAs near threshold, at various temperatures. As the temperature increases the band gap decreases, basically because of the thermal expansion of the lattice (Appendix 2.3). The peak is caused by absorption leading to the creation of excitons and is more prominent at low temperature: if kT is of the order of the exciton binding energy, broadening of the peak will become significant.

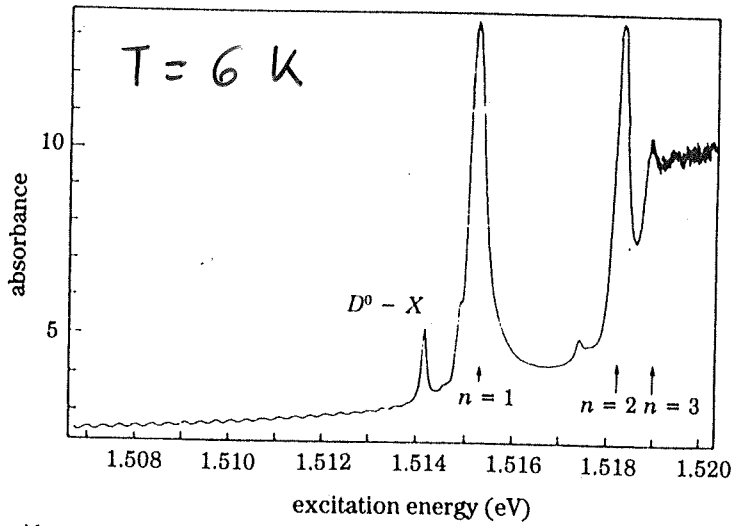

GaAs

Fig. 6.5. Absorption measured at $T = 6$ K of a sample of pure GaAs containing residual donors. The absorbance is proportional to the absorption coefficient α. Note the peaks corresponding to the levels $n = 1, 2$, and 3 of the exciton, as well as a peak associated with an exciton bound to a neutral donor ($D^0 - X$).

GERMANIO

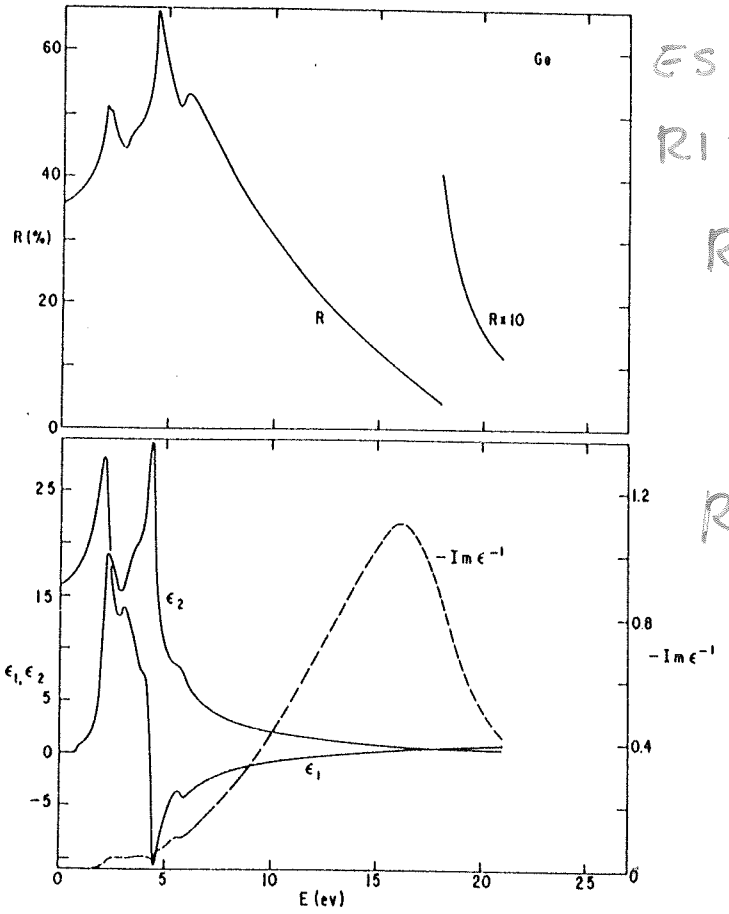

ESPERIMENTO DI RIFLETTIVITA'

$$R = \left|\frac{\varepsilon_2}{\varepsilon_1}\right|^2$$

$R \rightarrow \varepsilon_1, \varepsilon_2$

Fig. 5.7 Room-temperature reflectivity and optical constants of Ge. [From H. R. Phillip and H. Ehrenreich, *Phys. Rev.* **129**, 1550 (1963).]

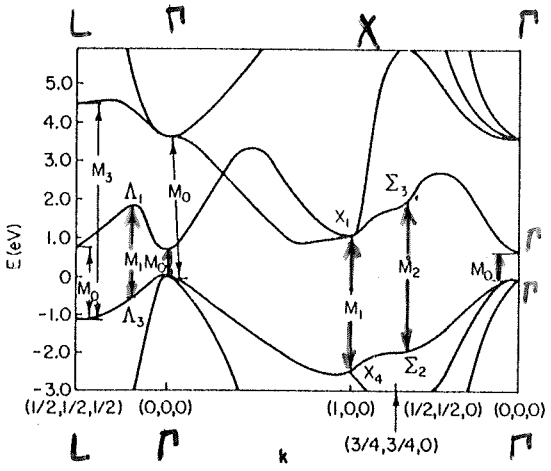

TEORIA

Fig. 5.8 The band structure of Ge. [From J. C. Phillips, D. Brust, and G. F. Bassani, *Proc. Int. Conf. Phys. Semicond. Exeter London* p. 564 (1962).]

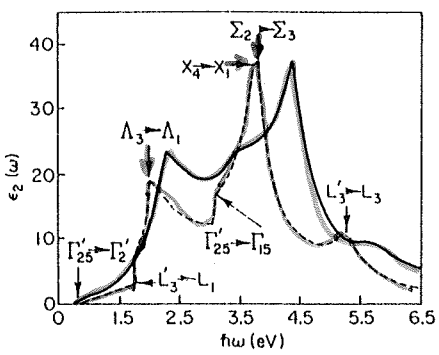

— ESPERIMENTO

— TEORIA

Fig. 5.9 Imaginary part of the dielectric constant $\varepsilon_2(\omega)$ for Ge. (——) Experiment; (–·–·–) theory. [From D. Brust, J. C. Phillips, and G. F. Bassani, *Phys. Rev. Lett.* 9, 94 (1962).]

$$I = I_0 e^{-\alpha x}$$

$$\alpha = \frac{\varepsilon_1 W_{is}}{nc} = \frac{\omega \varepsilon_2}{nc} \rightarrow \varepsilon_2 \sim \alpha$$

Gap diretta

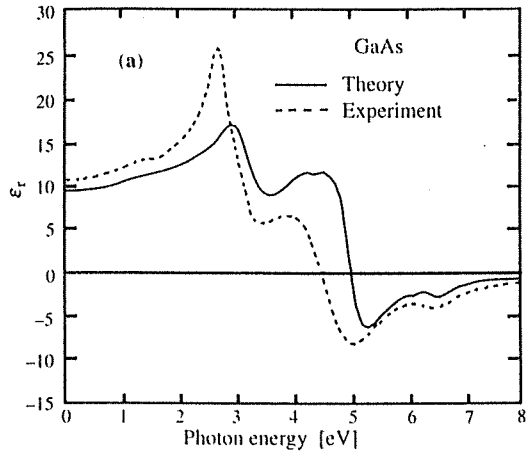

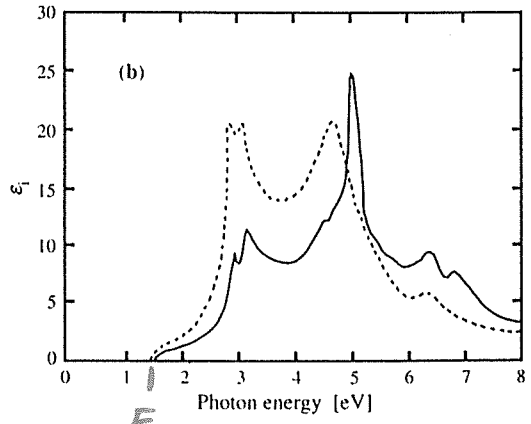

E_g

$E_g \sim 1.42$ eV

$\varepsilon_2 > 0$ per $\hbar\omega \geq E_g$

GAP INDIRETTA

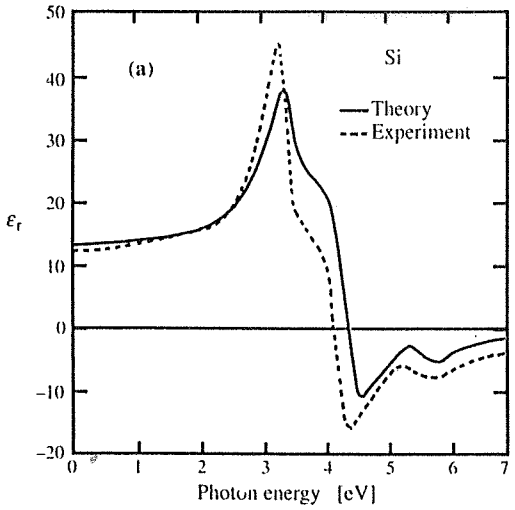

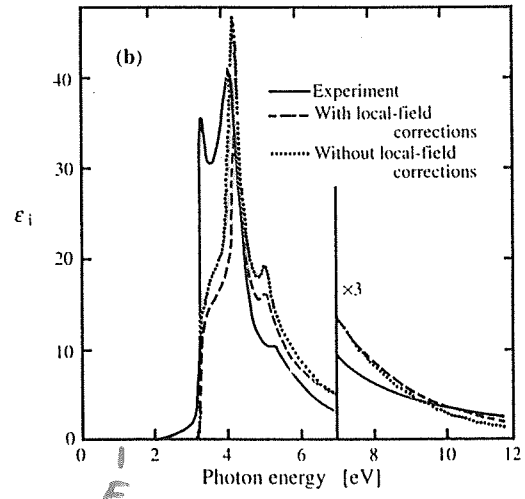

E_g

$E_g \sim 1.15$ eV

COSTANTE DIELETTRICA : METALLI

TEORIA

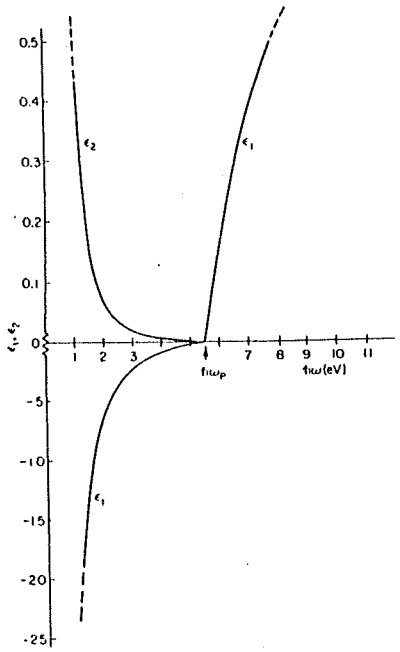

Fig. 3.8 Spectral dependence of ϵ_1 and ϵ_2 for a free-electron metal. The calculations are for the case in which $4\pi Ne^2/m = \omega_p^2 = 30$ eV^2 and $\hbar\Gamma = 0.02$ eV. Note the difference in scale of the ordinate along the positive and negative axes. The magnitude of ϵ_1 is much greater than that of ϵ_2 for the frequency range shown. For $\hbar\omega < \hbar\Gamma$, $|\epsilon_2/\epsilon_1| \to \Gamma/\omega$ and ϵ_2 dominates.

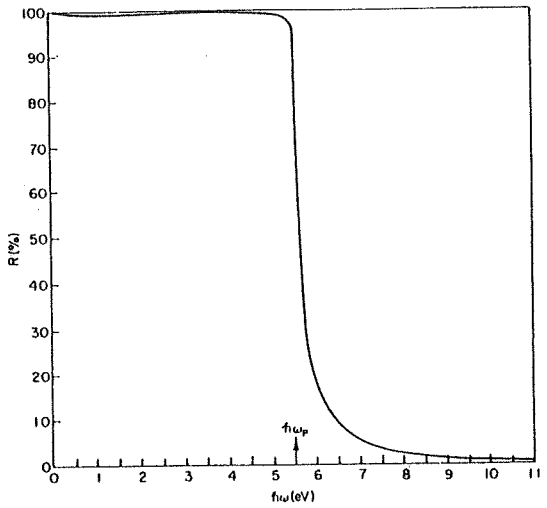

Fig. 3.11 Spectral dependence of reflectivity for a free-electron metal. The curve is calculated from the n and k values given in Fig. 3.9.

$$\epsilon_1 = 1 - \frac{\omega_p^2 \tau^2}{(1+\omega^2\tau^2)}$$ DRUDE

$$\epsilon_2 = \frac{\omega_p^2 \tau^2}{(1+\omega^2\tau^2)\omega}$$

Al

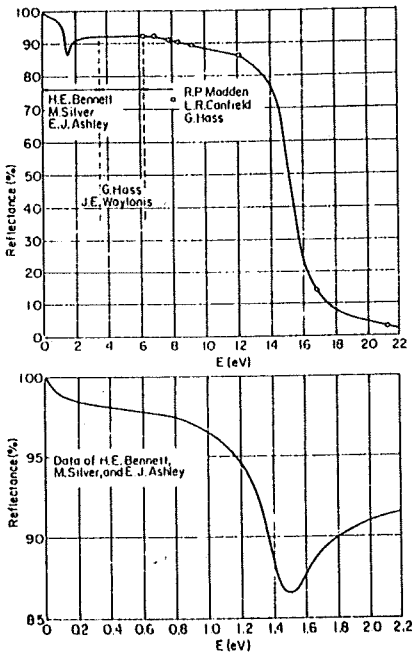

ESPERIMENTO

Fig. 3.13 Reflectance of aluminum. The decrease in reflectance at $\hbar\omega = 1.4$ eV arises from a weak interband transition. The large decrease in reflectance at $\hbar\omega = 14.7$ eV identifies the plasma resonance. [From H. Ehrenreich, H. R. Philipp, and B. Segall, *Phys. Rev.* 132, 1918 (1963).]

COSTANTE DIELETTRICA DI UN SEMICONDUTTORE

TEORIA

$\hbar\omega_0 = 4\,eV$

$\hbar\Gamma = 1\,eV$

$\frac{4\pi Ne^2}{\omega} = 60$

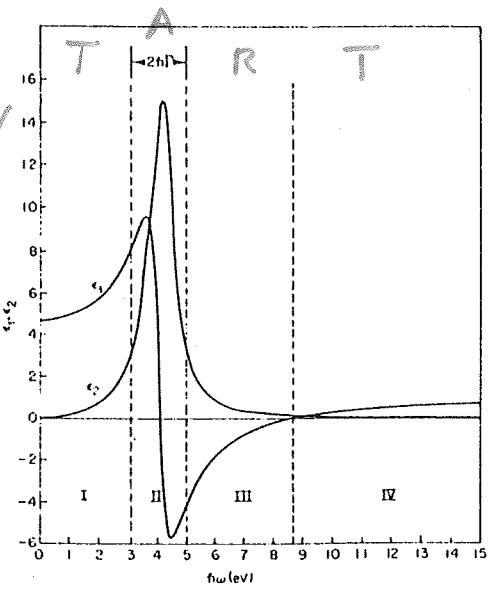

Fig. 3.3 Spectral dependence of ϵ_1 and ϵ_2. The curves are calculated for the case in which $\hbar\omega_0 = 4$ eV, $\hbar\Gamma = 1$ eV, and $4\pi Ne^2/m = 60$. The onset of region IV is defined by $\epsilon_1 = 0$.

$$\varepsilon_1 = 1 + \frac{4\pi Ne^2}{\omega}\,\frac{\omega_0^2-\omega^2}{(\omega_0^2-\omega^2)^2+\Gamma^2\omega^2}$$

$$\varepsilon_2 = \frac{4\pi Ne^2}{\omega}\,\frac{\Gamma\omega}{(\omega_0^2-\omega^2)^2+\Gamma^2\omega^2}$$

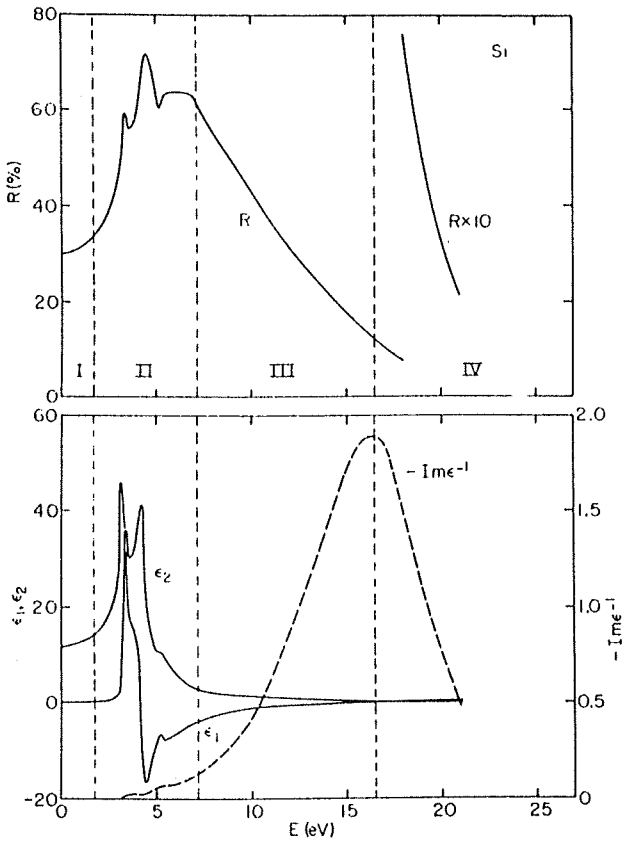

Fig. 3.7 The spectral dependence of the reflectance and dielectric functions of Si. Regions I, II, III, and IV correspond to the regions with the same designation shown in Figs. 3.1, 3.3, and 3.4 [H. R. Philipp and H. Ehrenreich, *Phys. Rev.* **129**, 1550 (1963).]

ESPERIMENTO

I: $\omega \ll \omega_0$ $\quad \varepsilon_2 = 2nk \approx 0$

$\varepsilon_1 = n^2 - k^2 > 1$

$\downarrow$

$k = 0$ $\quad \varepsilon_1 \sim n^2$

$n \sim A + B/\lambda^2$ Cauchy (prisma!)

SINGOLARITA' VAN HOVE

$$J_{cv} = \frac{1}{8\pi^3} \int \frac{dS}{|\vec{\nabla}_k E_{cv}|_{E_{cv} = \hbar\omega}}$$

MINIMO

PUNTO SELLA

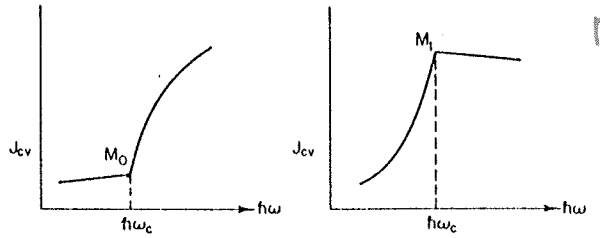

PUNTO SELLA

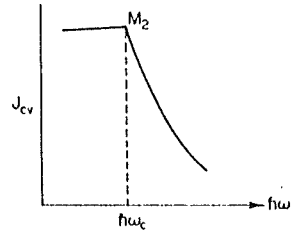

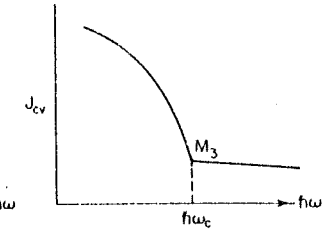

MASSIMO

Fig. 5.5 Van Hove singularities in the joint density of states J_{cv}. These singularities appear superimposed on a (sometimes) rather smooth background in J_{cv} arising from the totality of transitions throughout the Brillouin zone. Thus, e.g., the line sloping slightly down and to the left from M_0 represents the smooth background in the neighborhood of M_0. The figures are drawn such as to emphasize the critical point structure; the true zero in J_{cv} would generally be well off scale in these figures.

TABLE 5.1 *Joint Density of States J_{cv} for Critical Points*

Critical point	Type	β_1	β_2	β_3	J_{cv}	
					$\delta < \delta_0$	$\delta > \delta_0$
M_0	Minimum	+	+	+	0	$C_0(\delta - \delta_0)^{1/2}$
$M_1 (= S_1)$	Saddle point	+	+	−	$C_1 - C_1'(\delta_0 - \delta)^{1/2}$	C_1
$M_2 (= S_2)$	Saddle point	+	−	−	C_2	$C_2 - C_2'(\delta - \delta_0)^{1/2}$
M_3	Maximum	−	−	−	$C_3(\delta_0 - \delta)^{1/2}$	0

$$\varepsilon_2 = 8\left(\frac{\pi e}{m\omega}\right)^2 |\hat{a}_0 \cdot \vec{P}_{ij}|^2 J_{cv}$$

$\vec{\nabla}_k E_{cv} = 0 \Longrightarrow$ SINGOLARITA' DI VAN HOVE

ECCITONI

$$-\frac{\hbar^2}{2M}\nabla_R^2\psi(R) = E_R\,\psi(R)$$ moto CM eccitone

$$M = m_e^* + m_h^*$$

$$\left(-\frac{\hbar^2}{2\mu}\nabla_r^2 - \frac{e^2}{\varepsilon r}\right)\phi_n(r) = E_n\,\phi(r)$$

$$R = \frac{m_e^* R_e + m_h^* R_h}{m_e^* + m_h^*}$$

$$\frac{1}{\mu} = \frac{1}{m_e^*} + \frac{1}{m_h^*}$$

$$\bar{r} = \bar{R}_e - \bar{R}_h$$

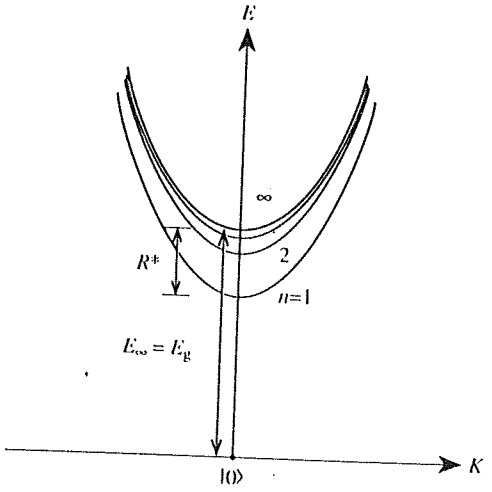

Fig. 6.21. The energy states of a Wannier exciton showing both its bound states $n = 1$ to 3 and the continuum states. E_g is the bandgap and R' the exciton binding energy

$= 13.6\,eV$

$$E = E_g - \frac{\mu}{m}\frac{E_1}{\varepsilon^2 n^2} + \frac{\hbar^2 K^2}{2M}$$

$n = 1, 2 \ldots$

$$\bar{K} = \bar{k}_e + \bar{k}_h$$

Table 6.4. Exciton binding energy (R') and Bohr radius (a_0) in some direct bandgap semiconductors. The three semiconductors labeled (W) have the wurtzite crystal structure while the others have the zinc-blende structure. Experimental values of R' and a_0 are from [Ref. 6.40, p. 155, 41]. The theoretical values of R' are from [6.38]

Semiconductor	R' [meV]	R' (theory) [meV]	a_0 [Å]
GaAs	4.9	4.4	112
InP	5.1	5.14	113
CdTe	11	10.71	12.2
ZnTe	13	11.21	11.5
ZnSe	19.9	22.87	10.7
ZnS	29	38.02	10.22
ZnO (W)	59		
CdSe (W)	15		
CdS (W)	27		